Co-expression of calcium channels and delayed rectifier potassium channels protects the heart from proarrhythmic events

Sara Ballouz[a,1], Melissa M Mangala[b,1], Matthew D Perry[b,c,1], Stewart Heitmann[b], Jesse A Gillis[a], Adam P Hill[b,c,2], Jamie I Vandenberg[b,c,2]

Author Affiliation:

a. Stanley Institute for Cognitive Genomics, Cold Spring Harbor Laboratory, Woodbury, NY 11797, USA.
b. Victor Chang Cardiac Research Institute, Darlinghurst, NSW 2010, Australia
c. University of NSW, Sydney. Kensington, NSW 2052, Australia

1. These authors contributed equally to this study

2. Corresponding Authors:

Jamie I Vandenberg* and Adam P Hill†,
Victor Chang Cardiac Research Institute,
Lowy Packer Building, 405 Liverpool Street
Darlinghurst, NSW 2010
Australia

* j.vandenberg@victorchang.edu.au
† a.hill@victorchang.edu.au

Abstract (140 words)

Cardiac electrical activity is controlled by the carefully orchestrated activity of more than a dozen different ion conductances. Yet, there is considerable variability in cardiac ion channel expression levels both within and between subjects. In this study we tested the hypothesis that variations in ion channel expression between individuals are not random but rather there are modules of co-expressed genes and that these modules make electrical signaling in the heart more robust.

Meta-analysis of 3653 public RNA-Seq datasets identified a strong correlation between expression of *CACNA1c* (L-type calcium current, I_{CaL}) and *KCNH2* (rapid delayed rectifier K^+ current, I_{Kr}), which was verified in mRNA extracted from human induced pluripotent stem cell-derived cardiomyocytes. *In silico* modeling indicates that the co-expression of *CACNA1c* and *KCNH2* limits the variability in action potential duration and reduces susceptibility to early afterdepolarizations, a surrogate marker for pro-arrhythmia.

Keywords:

Ion channels; co-expression; gene modules; meta-analysis; cardiac action potential, early afterdepolarization, arrhythmia, drug-induced long QT syndrome

Introduction

Robust electrical signaling in the heart is critical for co-ordinating the efficient pumping of blood around the body. Failure of cardiac electrical signaling, even for just a few minutes, can have fatal consequences, with sudden cardiac death accounting for up to 10% of deaths in our community (1). Despite decades of research, predicting in advance who is more or less susceptible to sudden cardiac death remains challenging (2).

The action potential (AP) of excitable cells, such as cardiac myocytes and neurons, reflects the orchestrated activity of at least a dozen distinct ion channels and electrogenic transporters (3) (4). In such complex systems, both theoretical and experimental studies have shown that there is considerable inter-individual variability in the combinations of molecular input parameters that can produce very similar integrated outputs (5) (6). This has led to a paradigm shift in computational modeling that relies not on generating idealized outputs based on mean data but rather development of populations of models that account for the observed variability in molecular inputs (7) (8). Such models are already proving useful for interrogating inter-individual variability in response to pathological stimuli (9) (10) (11). Our challenge now is to discern the underlying essence of these complex systems (12,13) so that we may then make rational interventions to treat pathology that takes into account inter-individual variation. Specifically, are there underlying principles regulating cardiac electrical activity that can provide insights into why some people are more susceptible to sudden cardiac death in response to pathological

stimuli, such as drug block of the rapid delayed rectifier potassium channel (I_{Kr}) which is the underlying basis of drug-induced long QT syndrome (di-LQTS) (14).

A common approach to discern patterns in multi-dimensional biological problems has been to look for co-expression networks (13) (15). Co-expression networks are known to encode functional information (16), with co-expression reflecting co-regulation and co-functionality (17) (18). To help identify robust co-expression modules, it is helpful to use meta-analytical approaches, as the aggregation of large numbers of individual networks across multiple independent experiments averages away noise and reinforces those correlations that reflect real signals (19) (20) (21).

Here, we have used meta-analytic co-expression analysis in large scale human gene expression data sets to identify modules of co-expressed ion channel genes which were then used to constrain population models of cardiac electrical activity. These models were then used to test the hypothesis that co-expression of repolarization and depolarization currents helps prevent irregular action potentials from emerging when human cardiac myocytes are exposed to pro-arrhythmic stimuli. We show that tight coupling of current densities for the L-type calcium current (I_{CaL}) and the rapid component of the delayed rectifier potassium current (I_{Kr}) reduced the emergence of pro-arrhythmic early afterdepolarizations (EADs) and this protection persisted in the face of highly variable expression of other ion channels, as well as in the presence of pharmacological block of I_{Kr}, a potent pro-arrhythmic stimulus (22). A very important prediction to arise out of our modelling studies is that in the context of drug block of I_{Kr} those patients with high expression of I_{CaL} and I_{Kr} experience more EADs and are therefore more likely to be susceptible to ventricular arrhythmias.

Results

The shape and duration of action potentials in cardiac myocytes are determined by the orchestrated activity of voltage-gated sodium, calcium and potassium channels, as well as a series of electrogenic transporters that regulate intracellular ion concentrations (See Supplementary data **Figure S1**). These channels, transporters and related intracellular calcium handling proteins are encoded by a few dozen genes, sometimes referred to as the rhythmonome (23) (see Supplementary data, **Table 1**).

To determine whether there were any co-expression patterns among the rhythmonome genes we first undertook an untargeted screen for possible expression correlation patterns in publicly available RNA-seq data sets (see list of RNA-seq experiments in supplementary data, **Table 2**). Ranked correlation coefficients from an aggregate co-expression network that contain data from 3653 samples are illustrated in the heatmap in **Figure 1A**. High ranked correlations indicate similarity of transcriptional profiles between the genes. A clustering analysis, as shown by the dendrogram in **Figure 1A**, groups genes according to their correlation similarities, as defined by the Spearman's correlation coefficients (see

color code in **Figure 1A**). There is a large cluster of yellow/green squares in the bottom left corner indicating that there are significant levels of correlation amongst many of the genes. Furthermore, within this large cluster there are two sub-clusters. The cluster of yellow-green squares corresponding to 13 genes in the bottom left corner (red dashed box in **Figure 1A**) encode for proteins that regulate calcium fluxes as well as the transient outward K^+ current (*KCND3*), which helps to maintain the plateau potential at a level that maximizes calcium influx (24). A second sub-cluster, in the upper right quadrant of the main cluster, encompasses 10 genes (black dashed box in **Figure 1A),** including *KCNH2, SCN5a, KCNJ12* and *KCNIP2*, that encode for ion channel proteins important for regulating action potential duration (APD).

Overall, the connectivity within the set of rhythmonome genes is fairly high in comparison to their connectivity to all other genes in the co-expression network (node degree analysis, p~5.7e-14), with a central gene being *CACNA1C*, the gene encoding the alpha subunit of the L-type calcium channel (see Supplementary data, **Figure S2**). Although *CACNA1c* clusters in the group of calcium handling genes in the bottom left quadrant of the main cluster in **Figure 1A**, it also shows high levels of correlation with the cluster of ion channel genes in the top right quadrant of **Figure 1A**. In a similar fashion, the *KCNH2* gene, which encodes for I_{Kr}, is included in the ion channel cluster but also shows moderate-high correlations with a portion of the calcium handling genes in the bottom left quadrant. The highest ranked co-expression partners for *CACNA1C* and *KCNH2* are highlighted in **Figure 1B.**

The vast majority of the public RNA-Seq datasets included in our analyses were not heart specific. It is, however, noteworthy that there are no strong correlations between the expression of any of the individual ion channel or calcium handling genes and the cardiac-specific markers included in our analyses: *GATA-4*, *NKX2-5*, *MYL2* and *MYL7*. For example, the cardiac marker genes are towards the bottom of the lists in **Figure 1B**. This suggests that the correlations within the set of rhythmonome genes are not simply a reflection of cardiac specific expression but rather represent intrinsic correlations.

Figure S1: *In silico* model of ventricular Action Potential

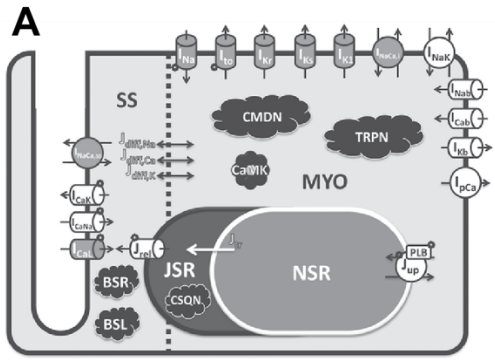

B

Conductance parameter	scalar
GKs	8.09
GKr	1.17
GCaL (PCa)	3.57
PNaCa (Gncx)	3.05
PNaK	1.91
GNaL	1.7

A. Schematic diagram of the ventricular myocyte model used in this study (reproduced from (25) under the CC-BY licence.
B. Scaling factors applied to the original model were taken from (26)

Figure 1: Cardiac ion channel and calcium handling protein co-expression connectivity analysis from published RNA-seq datasets

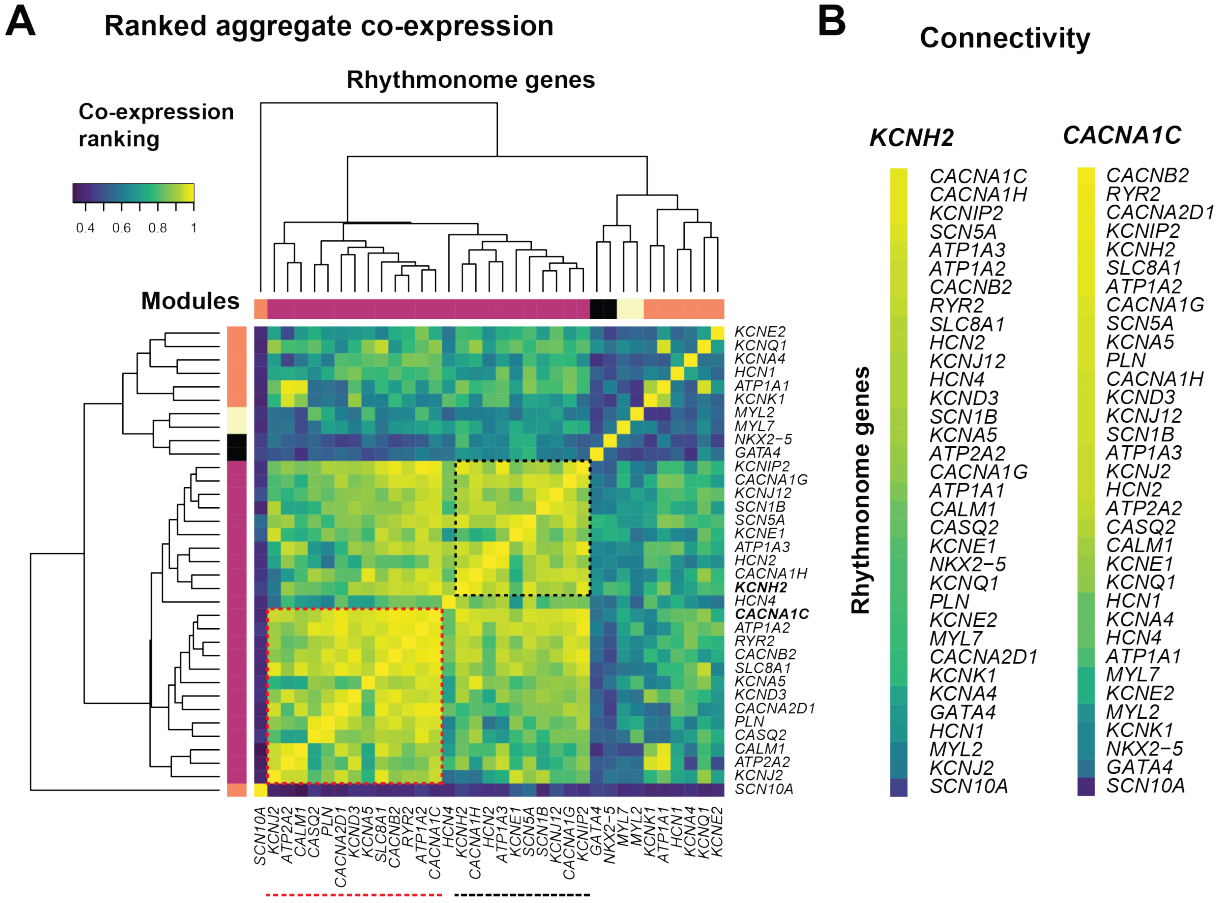

A. Sub-network of co-expression ranking across 35 genes encoding for cardiac ion channels or calcium homeostasis proteins (see Supplementary Table 1). Blue: low ranked correlations, yellow: high ranked correlations. The dendrogram illustrates the modules of genes with high levels of similarity in their transcriptional profiles. Red and black dashed boxes highlight subnetworks of correlated genes **B**. Connectivity of genes to *KCNH2* (encodes for I_{Kr}) and *CACNA1C* (encodes for I_{CaL}).

152 **Figure S2: Network connectivity for each rhythmonome gene**

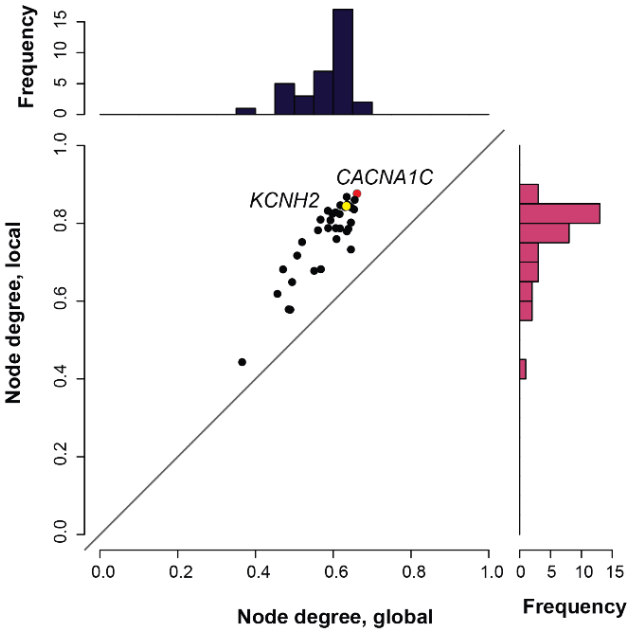

153
154 The degree of network connectivity for each rhythmonome gene within the local
155 rhythmonome network (y-axis) versus its connectivity within the whole genome (x-axis).
156 All the rhythmonome genes are more highly connected within the local network (i.e., all
157 the points lie above the line of identity, $p \sim 5.7e^{-14}$). *CACNA1C* is highlighted in red and
158 *KCNH2* in yellow.

159 To investigate whether the meta-analytic co-expression patterns observed in **Figure 1**
160 were also seen in human heart cells, we extracted mRNA from human induced pluripotent
161 stem cell-derived cardiomyocytes (hiPSC-CMs) (27) obtained from 10 patients with no
162 known heart disease**.** All samples contained high levels of cardiac marker genes (*MYL7,*
163 *GATA4* and *NKX2*.5) **(Figure 2A)**. Furthermore, the levels of expression of the housekeeper
164 genes, *GPADH* and *HRPT1* were similar across samples (see data at right side of **Figure 2A**).
165 The levels of expression of most rhythmonome genes showed variations between the
166 samples that spanned approximately an order of magnitude. However, similar to the
167 generic tissue RNA-Seq datasets, there were modules of co-expressed genes (e.g., see
168 dashed box in bottom left quadrant of **Figure 2B**). Most of the 13 genes in the cluster in
169 **Figure 2B** are present in the modules highlighted by the black and red dashed boxes in
170 **Figure 1A**. Conversely, many of the ion channel genes contained in the modules
171 highlighted in **Figure** 1 are not present in the module in **Figure 2** (e.g. *KCNJ2/KCNJ12*,
172 which encodes for I_{K1}; *KCND3*, which encodes for I_{To}; and *SCN5a*, which encodes for I_{Na}).
173 These genes are all known to be expressed at lower levels in embryonic hearts and so
174 unsurprisingly they are not well expressed in the hiPSC-CM lines (28).

175 We next looked to see if there were any specific relationships between genes encoding
176 depolarization and repolarization currents, within the hiPSC-CM expression profiles. In
177 **Figure 2C,** we have plotted the expression of *KCNH2* versus the genes that encode for the
178 depolarization currents that showed the highest levels of correlation with expression of
179 *KCNH2* in the generic tissue datasets (see **Figure 1B**, i.e., *CACNA1c*, *CACNA1H* and *SCN5a*).

The most notable correlation that was observed in the hiPSC-CMs was that between *KCNH2* and *CACNA1c*; $r^2 = 0.89$ (**Figure 2C**).

As the only robust relationship that we observed in both the generic tissue sets and the hiPSC-CM lines was the co-expression of *KCNH2* and *CACNA1c*, we focused on this pair for our subsequent studies. To investigate whether co-expression modules of ion channel genes might influence integrated cardiac electrical function, we used an *in silico* approach. First, we simulated a population of 1000 human cardiac action potentials where random scalar values, chosen from a log normal distribution with mean 1 and standard deviation of 0.5 (**Figure 3A**, lower panel), was applied to every conductance in each iteration of the action potential model (see **Figure 3A** and Supplementary Data, **Movie S1**).

Figure 2: HiPSC-CM mRNA correlation analysis

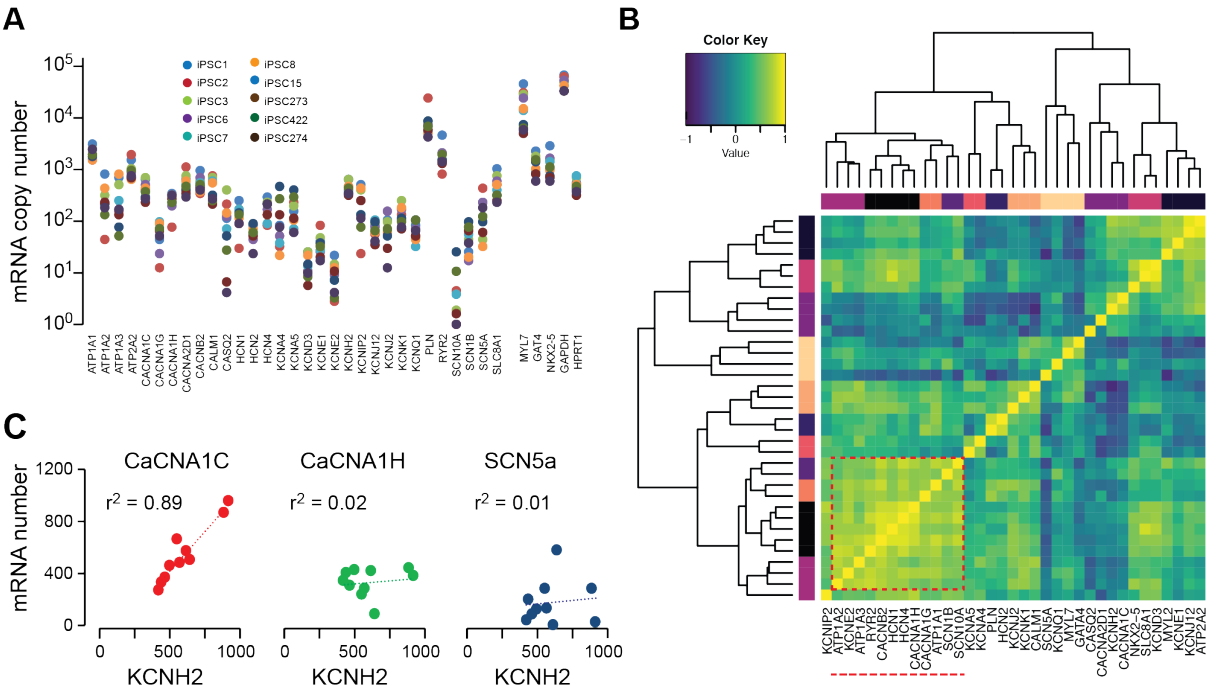

A. plot of all mRNAs (log axis) for 10 hiPSC-CM lines. Note that there are high levels of expression of cardiac markers (*MYL7* as well as *NKX2-5* and *GATA4*) in all cell lines. Also there is less variability in the levels for the housekeeping genes (*GAPDH* and *HPRT1*) compared to that seen for the ion channels and calcium handling proteins. **B.** Correlation matrix for hiPSC-CM mRNA. The red dashed box highlights the module with the highest correlations. **C.** Correlation plots for *KCNH2* versus genes that encode the major depolarizing currents (*CACNA1c*, *CACNA1H* and *SCN5a*).

The baseline action potential produced by this model (black trace in right hand panel of **Figure 3A**) has a duration at the point of 90% repolarization (APD_{90}) of 264 ms. The population of 1000 cardiac cells generated by randomly scaling the conductances exhibited APD_{90} values that ranged from ~120 ms to ~500 ms (**Figure 3A,** right panel, and **Figure 3B**). We next selected those cells with APD_{90} values that fell within 20% of the mean value

(red bars, **Figure 3B**) to determine if there were any patterns of ion channel co-expression that could contribute to keeping the APD_{90} within this narrow selected range. The correlation matrix of the conductance scaling factors for the selected cells (**Figure 3C**) reveals a positive correlation between G_{Kr} and G_{CaL} (R=0.36) as well as an inverse correlation for G_{Kr} and G_{Ks} (R=-0.46). The positive correlation between the conductance scalars G_{Kr} and G_{CaL} in the *in silico* modelling dataset (**Figure 3**) suggests that the correlation seen between *CACNA1c* and *KCNH2* mRNA expression in both the public RNA-Seq datasets (**Figure 1**) and the hiPSC-CM dataset (**Figure 2**) would contribute to reducing the population variability in APD_{90} values.

We next repeated our previous simulation of 1000 action potentials but forced the conductance scaling factors for I_{Kr} and I_{CaL} to be identical in each cell (denoted co-expression in **Figure 4,** also see Data supplement, **Movie S2**). The scaling factors for all other conductances remained independent. The distribution of APD_{90} values for both independent and co-expression cell populations becomes broader as the level of variability is increased (**Figure 4A-C**). However, the spread of APD_{90} values in the cells with identical G_{CaL}-G_{Kr} scalars is always narrower than in the cell populations with independent G_{CaL}-G_{Kr} scalar values. For example, in the case of **Figure 4B,** the variance of the APD_{90} values was 0.026 for the co-expression dataset but 0.046 for the independent dataset (see supplementary data **Figure S3-C**). Another notable feature of the data in **Figure 4C** is that early afterdepolarisations (EADs) begin to appear in the cell population with independent scalars when the scalar variability, σ^2, exceeds 0.20 (also see supplementary data **Figure S4**). The number of cells with an EAD are indicated in parentheses above each distribution in **Figure 4C.**

Figure 3: *In silico* predictions of conductance scalars that give APD_{90} values in the normal range

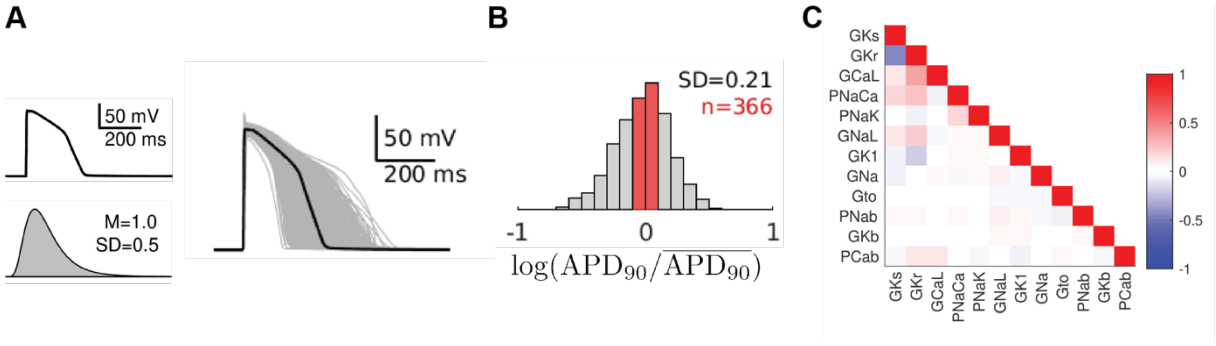

A. Baseline AP model and frequency histogram of scalars (log normal distribution with a mean of 1 and SD of 0.5) used to generate the population of 1000 APs with the baseline AP (all scalars set to 1.0) shown in black. **B.** Frequency histogram of APD_{90} values for the 1000 simulations with those falling within ±20% of the mean value shown in red. **C.** correlation matrix for sets of conductance scalars that gave APD_{90} values within ±20% of the mean value

Figure 4: Impact of I_{Kr}-I_{CaL} co-expression and conductance scalar variability on APD90 variability

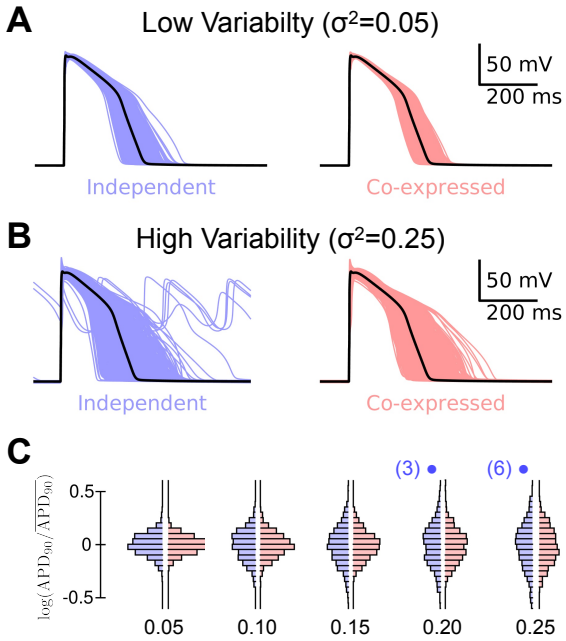

Raw APs for independent (blue) and co-expression of G_{Kr}-G_{CaL} (red) for **A.** low scalar variability (σ^2=0.05) and **B.** high scalar variability (σ^2=0.25). Note the presence of EADs in 6 of the APs in the independent group with σ^2 = 0.25. **C.** Histograms of log(APD_{90}/mean APD_{90}) distributions for co-expressed (red) or independent (blue) G_{Kr}-G_{CaL} simulations with σ^2 = 0.05, 0.1, 0.15, 0.2, 0.25. The numbers in parentheses above the 0.2 and 0.25 groups indicate the number of EADs in each independent scalars group.

Movie S1

Movie S2

Figure S3: Population models of ventricular APs with different levels of scalar variance

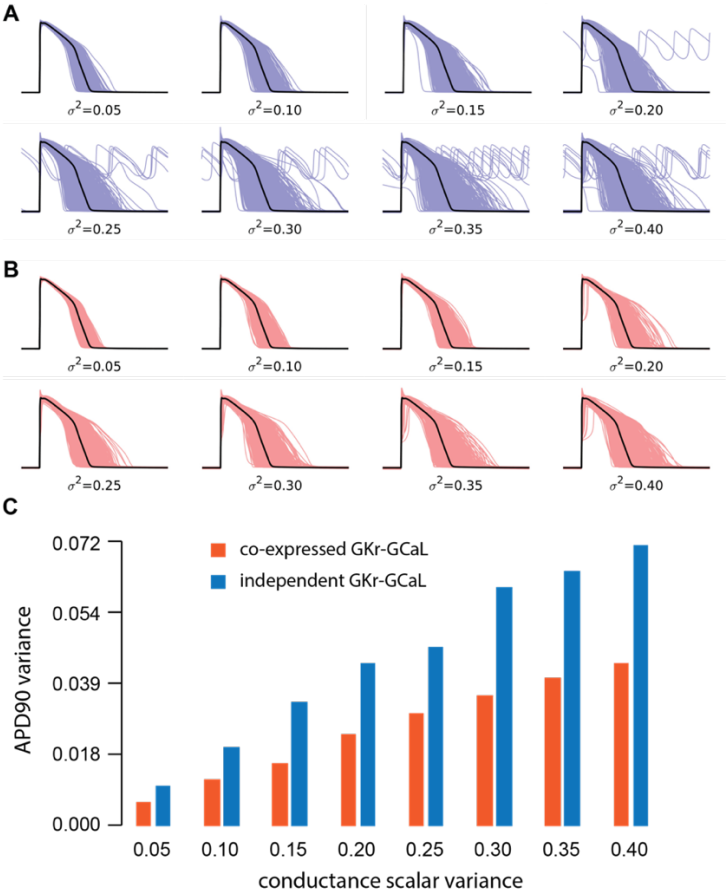

A-B. Population of models with variance systematically increased from σ2 = 0.05 to 0.40 for independent conductance scalars for G_{Kr} and G_{CaL} **(A), or** co-expression conductance scalars for G_{Kr} and G_{CaL} **(B)**. As the variance increases, the number of cells that develop EADs increases in the independent series. Conversely, for the co-expression models, there are no EADs even at variances up to 0.4. **C.** Variance of the APD_{90} distributions for each set of conductance scalar inputs for independent (blue) and co-expression (red) of I_{Kr} and I_{CaL}. Note that the variance of the APD90 distribution was always greater for the independent simulations ($p<0.008$ between groups, paired t-test)

We next investigated whether coupling of the conductance scalars for G_{Kr} and G_{CaL} influenced the generation of EADs in response to a pathological stimulus. Specifically, how cells respond to drug block of I_{Kr}, the underlying cause of di-LQTS (22). Example populations of action potentials obtained for independent and co-expression populations with I_{Kr} block of 0%, 50% and 80% are illustrated in **Figure 5.** As the extent of I_{Kr} block is increased (from A to C), the proportion of simulated action potentials producing EADs increases. It is also clear that at lower levels of I_{Kr} block, EADs were more frequent when G_{CaL} and G_{Kr} scalars were modulated independently (see **Figure 5B** and inset to **Figure 5D**). However, the proportion of simulations developing EADs in both the independent and co-expression populations becomes similar when the extent of I_{Kr} block exceeds 80% (**Figure 5D**).

It is well established that only a subset of patients exposed to drugs that block I_{Kr} (29), or with a mutation causing 50% loss of I_{Kr} function (30), will develop life threatening arrhythmias. This is consistent with the prediction made by our simulated drug block experiments shown in **Figure 5**. We therefore asked whether the data from the co-expression datasets could tell us anything about what factors might predispose to the development of EADs in the presence of a drug that blocks I_{Kr}. Analysis of the subset of scalars within the co-expression dataset that produced the 50 longest APs without EADs, compared to the subset of scalars that resulted in APs with EADs, is illustrated in **Figure 6A and 6B** respectively. Notably, the longest APs without EADs had low G_{CaL} scalars (and hence low G_{Kr} scalars) before addition of drug block. Conversely, the APs that developed EADs had higher G_{CaL} and G_{Kr} scalars. In **Figure 6C**, we have plotted the APD_{90} values for cells in the highest (red) and lowest (blue) quartiles of G_{Cal} - G_{Kr} scalars. As expected, the low G_{CaL} group showed longer APD_{90} values on average compared to the high G_{CaL} group (see the continuous lines in **Figure 6C**). Furthermore, for the 70% I_{Kr} block scenario, 44% of the high G_{CaL} group have developed EADs whereas only 7% of the low G_{CaL} group have developed EADs (compare red and blue bars at 70% drug block in **Figure 6C**). Thus, higher G_{CaL} is associated with a greater risk of developing EADs in response to moderate levels of I_{Kr} block. A similar pattern of results was observed when G_{CaL} and G_{Kr} were allowed to vary independently, except that in this scenario the difference between the high G_{CaL} and low G_{CaL} groups was even more dramatic at lower levels of I_{Kr} block (see supplementary data **Figure S4**).

Figure 5: Impact of G_{Kr}-G_{CaL} co-expression on response to drug block of I_{Kr}

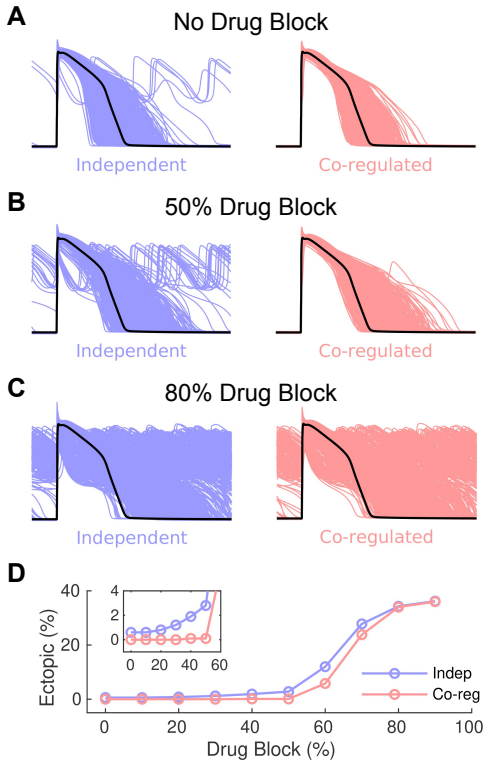

Raw APs for co-expressed G_{Kr}-G_{CaL} (red) and independent (blue) G_{Kr}-G_{CaL} populations, with scalar variance $\sigma^2 = 0.25$, for **A.** control, **B.** 50% I_{Kr} block and **C.** 80% I_{Kr} block. **D.** plot of % of AP simulations with EADs versus % I_{Kr} block (co-expression, red and independent, blue). The inset in panel D shows an expanded view of the % EADs at small levels of I_{Kr} block.

Figure 6: High G_{CaL} increases risk of EAD formation at moderate I_{Kr} block

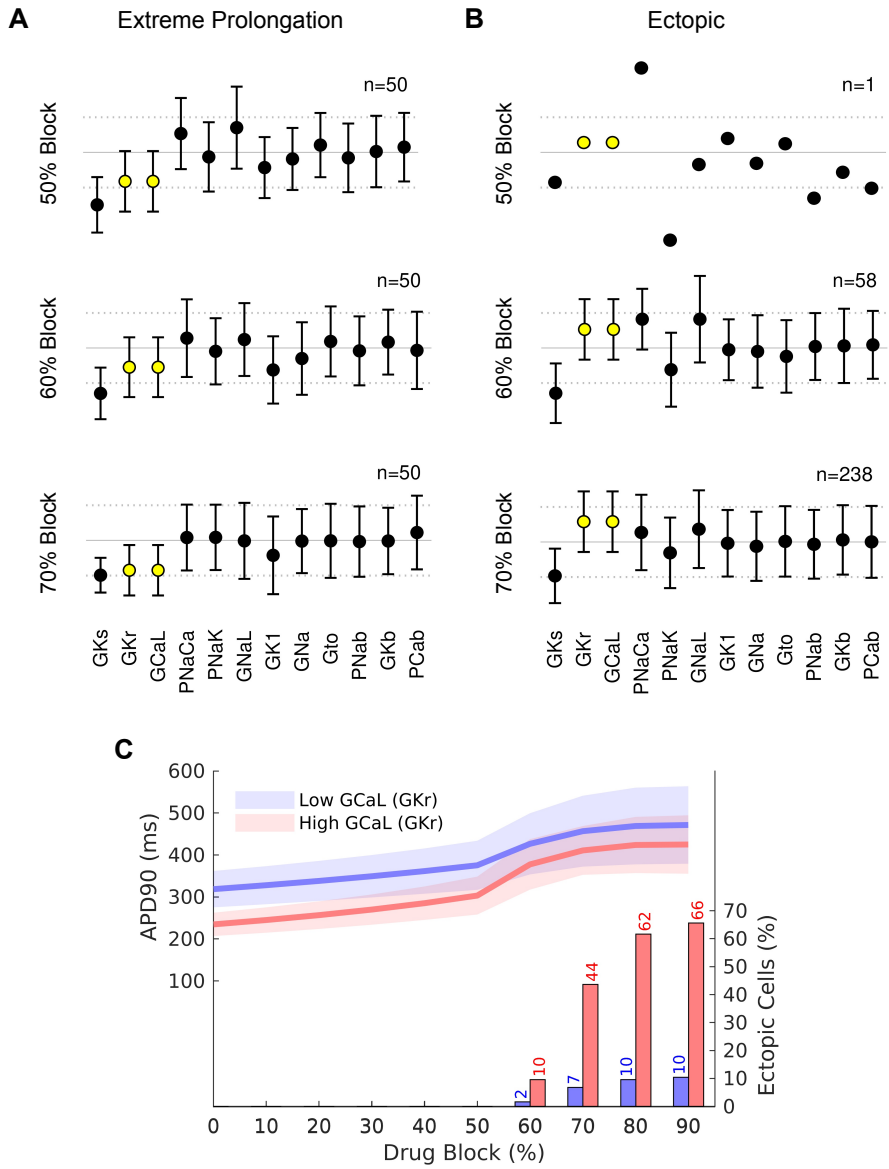

Scalars (box and whisker plots) for the population of cells with G_{Kr}-G_{CaL} co-expression. **A.** 50 cells with the longest APD_{90} values and no EAD with increasing % I_{Kr} block. **B.** scalars (box and whisker plots) for cells with EADs with increasing % I_{Kr} block. The G_{CaL} and G_{Kr} scalars are highlighted in yellow. **C.** APD_{90} values (left axis) for the highest (red) and lowest (blue) quartile of cells according to baseline G_{CaL} scalar. The continuous lines show the mean value and shaded area shows ±1 SD). The percentage of EADs in each quartile is shown as columns (see axis on right side of graph). The corresponding plots for the population of cells with independent G_{Kr}-G_{CaL} scalars are show in the Supplementary data (**Figure S4**)

Figure S4: High G_{CaL} increases risk of EAD formation at moderate I_{Kr} block even when G_{CaL} and G_{Kr} are varied independently

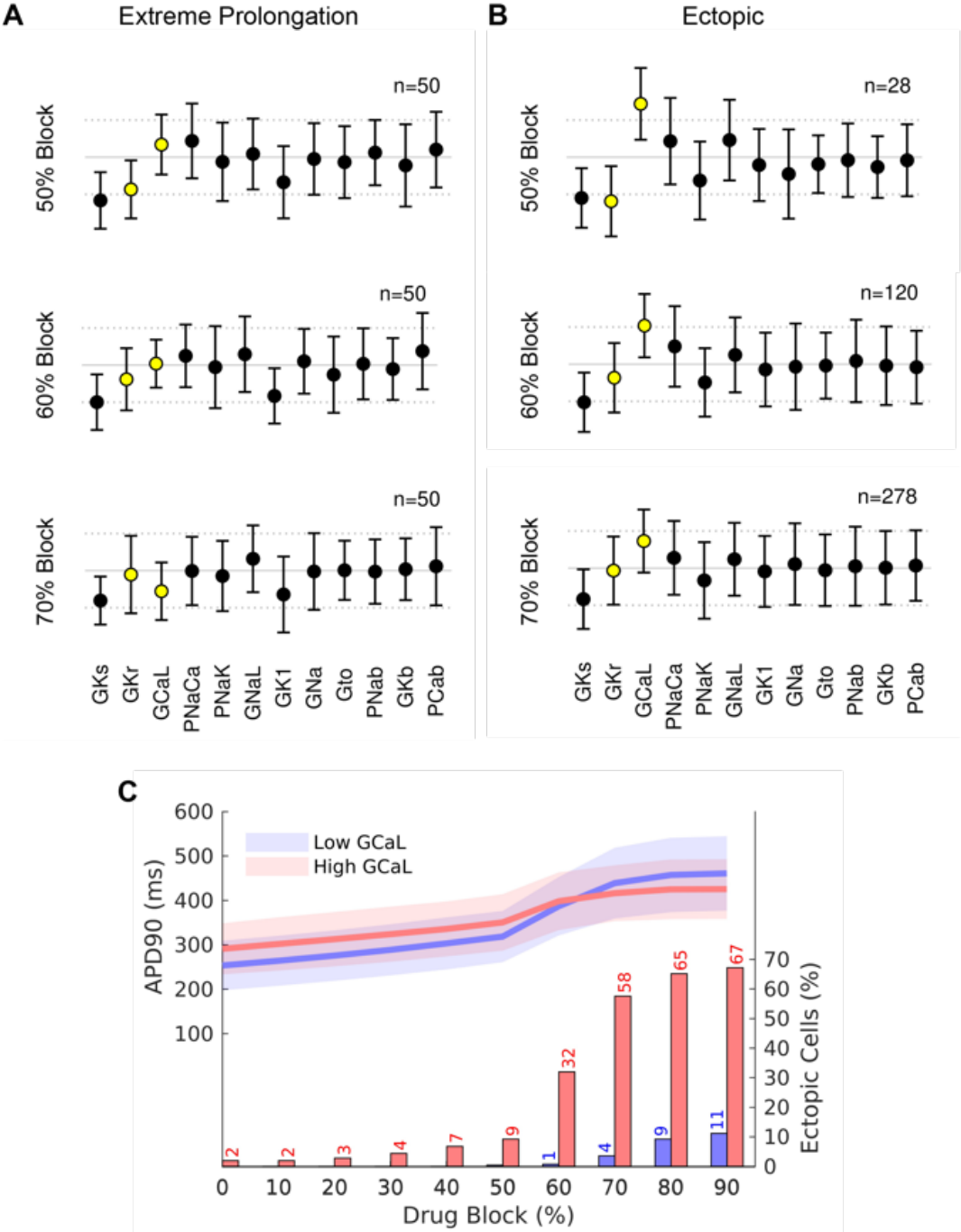

Conductance scalars (box and whisker plots) that give **A.** The 50 most extreme APD values or **B.** EADs for the population of cells with independent regulation of G_{Kr} and G_{CaL}. **C.** Plot of APD_{90} values for the highest quartile of G_{CaL} (red) and lowest quartile of G_{CaL} (blue) versus % drug block of I_{Kr}. The continuous line shows mean and shaded regions show ± 1 standard deviation. The column graph shows the % of cells that develop EADs at each level of drug block.

329 A corollary of our prediction that patients with high G_{CaL} are more susceptible to EADs
330 when exposed to a drug that blocks I_{Kr}, is that co-administration of a drug that blocks I_{CaL}
331 would reduce the incidence of EADs. Magnesium, which is used in the acute management
332 of di-LQTS (14), is a weak calcium channel blocker. Raising plasma [Mg^{2+}] from 1.5 to 2.5
333 mM would be expected to inhibit I_{CaL} by ~20% (31), conversely reducing [Mg^{2+}] from 1.5
334 to 0.5 mM would be expected to increase I_{CaL} by ~20%. When we increased I_{CaL} by 20%,
335 the incidence of EADs in the high G_{CaL} group increased from 10% to 16% for the 60% I_{Kr}
336 block simulation and from 44% to 58% for the 70% I_{Kr} block simulations (see **Figure 7)**. A
337 drug that inhibited I_{CaL} by 20% caused a modest decrease in the percentage of cells with
338 EADs and reduction of I_{CaL} by 50% had a correspondingly larger effect, for example,
339 reducing EADs from 44% to 12% in the 70% I_{Kr} block scenario (**Figure 7**).
340
341 **Figure 7: Effect of modifying I_{CaL} on incidence of EADs in response to I_{Kr} drug block.**

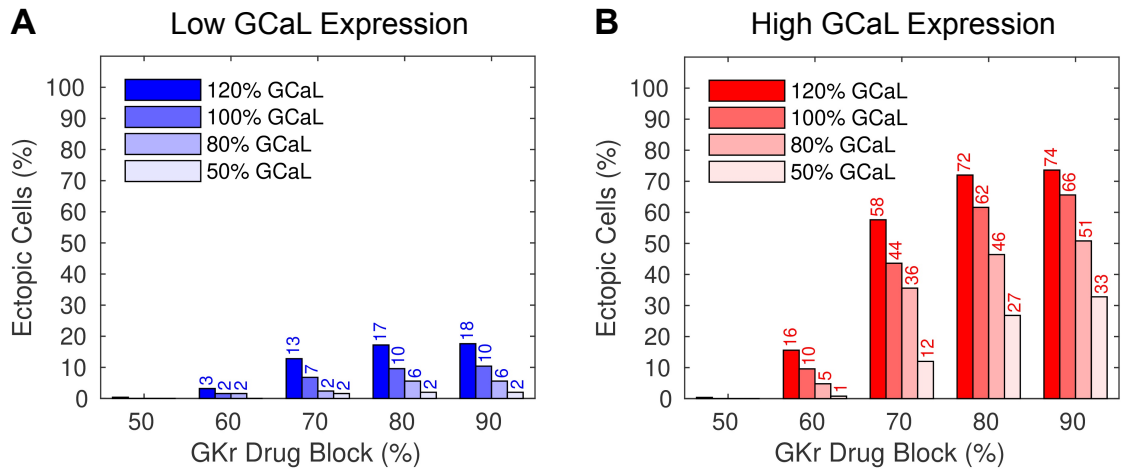

342
343 I_{CaL} was increased 20% to mimic hypomagnesaemia, reduced 20% to mimic
344 hypermagnesaemia (see text for details), or reduced 50% to mimic administration of a
345 calcium channel blocker. In both the quartile of cells with the lowest G_{CaL} scalars (blue, **A**)
346 and the quartile of cells with the highest G_{CaL} scalars (red, **B**) the incidence of EADs
347 increased when G_{CaL} was enhanced and decreased when G_{CaL} was decreased. The
348 observed differences were most pronounced with moderate (60-70%) I_{Kr} drug block.

349

350 **Discussion**

351 Cardiac electrical activity is regulated by the interdependent activity of a plethora of ion
352 channels, transporters and calcium handling proteins (4). Understanding the precise
353 details of how these conductances interact to control the rhythm of the heart has been an
354 enduring source of fascination. In this study, we have used meta-analytical techniques to
355 interrogate the large numbers of RNASeq datasets that have been deposited in public
356 access databases, to look for patterns of co-expressed genes that might help decipher the
357 control of cardiac electrical activity. The most important pair of co-expressed genes,
358 identified both in the public RNA Seq datasets (**Figure 1**) and in heart cells derived from

359 hiPSC lines (**Figure 2**), was that of *CACNA1c* (I_{CaL}) and *KCNH2* (I_{Kr}). Using an *in silico*
360 approach we demonstrated that tight co-expression of *CACNA1c* and *KCNH2*, against a
361 background of variability of all other ion channels, helps to control the duration of
362 repolarization (**Figure 4**). More importantly, the co-expression of *CACNA1c* and *KCNH2*
363 helps to protect the heart from early after depolarizations when they are exposed to drugs
364 that block I_{Kr} (**Figure 5**). Our simulations also suggest that inter-individual differences in
365 pro-arrhythmic responses to I_{Kr} drug block can be explained by inter-individual differences
366 in levels of *CACNA1c* expression (**Figure 6**).

367 Over the last few years, numerous groups have shown that there is considerable
368 heterogeneity of ion channel expression amongst excitable cells, including neurons (32)
369 and cardiac myocytes (7,19). Furthermore, since the pioneering work of Eva Marder and
370 colleagues, the presence of modules of co-expressed ion channel genes has also been well
371 appreciated(15). These previous studies, however, relied on patch clamp analysis of
372 isolated cells (15,33) and qPCR analysis (15) of individual ion channel mRNA, which are
373 highly laborious and so have been restricted to only a few important ion channel genes.
374 The advent of high throughput transcriptomic analyses has greatly facilitated the
375 identification of conserved networks of co-expressed gene modules amongst the entire set
376 of expressed genes (21). By applying meta-analytic approaches to a large number of
377 independent datasets one can more readily discern genuine co-expression signals from
378 noise, as well as explore smaller gene modules (21). In our analysis of a subset of
379 rhythmonome genes (35 members, **Table S1**) within a large library of public RNA Seq
380 datasets, (see **Table S2**) we identified two clusters of genes: a first subset that
381 predominantly affects calcium handling and a second subset that predominantly affects
382 membrane potential (see **Figure 1**). The nodes within each of these clusters that are most
383 closely connected within the rhythmonome relative to all other genes are *KCNH2* and
384 *CACNA1c* (**Figure S2**). This is analogous to a network of networks (34), where the *KCNH2-*
385 *CACNA1c* link provides an interconnection of the two networks. Independent evidence to
386 corroborate an important link between calcium handling and regulation of cardiac action
387 potential duration comes from the large genome-wide association studies (GWAS) of QT
388 interval duration which identified SNPs in a number of calcium handling genes as well as
389 *KCNH2* as being important determinants of QT interval in the population (35).

390 Due to the large number of associations we were testing for in our network analyses, it is
391 possible that some would occur by chance. That we were able to confirm the presence of
392 at least some of the co-expression modules in an independent dataset, i.e. the hiPSC-CM
393 (see **Figure 2**) provides important corroborative evidence that these co-expression
394 patterns are real and therefore likely to have physiological relevance. It should also be
395 noted that many ion channels important for function in adult cardiac myocytes are not
396 expressed at significant levels in immature cardiac myocytes, such as those derived from
397 hiPSC (e.g. *SCN5a, KCNQ1, KCNJ12, KCND3*, (28)). It is therefore possible that we have

398 underestimated the number of genes within the modules of co-expressed genes in adult
399 cardiac myocytes.

400 The patterns of co-expressed genes we observed show some important similarities, as well
401 as differences to previous studies. Banyasz et al. (33) and Rees et al. (18) have both
402 demonstrated that the expression of I_{CaL} is correlated with the sum of the major
403 repolarizing ion currents in guinea-pig and mouse respectively. However, the molecular
404 players involved in cardiac electrical activity in rodents are quite distinct to humans (36).
405 In humans, the most important determinant of repolarization duration at baseline is I_{Kr}
406 (37), whereas in guinea-pig I_{Ks} and I_{Kr} play equally important roles (33) and in mice the
407 fast component of the transient outward current ($I_{to,f}$) and the ultra-rapid delayed rectifier
408 (I_{Kur}) are the major repolarization currents (18). Thus, there is a common factor between
409 our study showing co-expression of *KCNH2* and *CACNA1c* in human and the previous
410 rodent studies, i.e., all studies show a correlation between I_{CaL} and the major repolarizing
411 currents present in that species. Our study, however, is the first to demonstrate the
412 important co-expressed genes in human heart tissue.

413 Identifying modules of co-expressed genes are the first step in seeking to understand the
414 logic of complex systems (6). Understanding how such modules impact function in health
415 and disease is the next challenge. In neuronal cells, Marder and colleagues have shown that
416 modules of co-expressed ion channels play an important role in regulating action potential
417 firing patterns (38). Rees and colleagues, have demonstrated that modules of co-expressed
418 depolarization and repolarization currents can help to ensure normal amplitude calcium
419 transients, a critical determinant of overall heart function (18). We have extended these
420 studies to show that in normal heart cells, co-expression of *KCNH2* (repolarization) and
421 *CACNA1c* (depolarization) channels help to maintain the plateau duration of the action
422 potential, which in turn likely contributes to regulating the duration and amplitude of the
423 calcium transient. More importantly, our studies provide the first insights into how
424 patterns of co-expressed ion channel genes influence the hearts response to pathological
425 stimuli.

426 Sudden death due to abnormalities of cardiac electrical signaling is a major cause of
427 mortality (1). Predicting in advance who is more or less susceptible to sudden cardiac
428 death and therefore warrants prophylactic treatment remains challenging (2). A key to
429 being able to predict who is at greatest risk is understanding why different people respond
430 differently to the same pro-arrhythmic stimulus. Based on the results of our *in silico*
431 studies, we have provided two important insights into the nature of interindividual risk for
432 developing arrhythmias in response to drugs that block I_{Kr}, the major cause of drug-
433 induced cardiac arrhythmias (14). First, cells with low G_{CaL} (and hence low G_{Kr} at baseline)
434 exhibited the greatest prolongation of AP duration when exposed to I_{Kr} drug block. Second,
435 cells with high G_{CaL} (and hence high G_{Kr} at baseline) showed greater propensity for
436 development of EADs at moderate levels of I_{Kr} drug-block (**Figure 6**). An important
437 implication of the observation that a high G_{CaL} increases the susceptibility to EADs in

438 response to drug block of I_{Kr} is that the co-administration of an I_{CaL} blocker should reduce
439 the risk of EADs (as shown in **Figure 7**). This is consistent with the observation that the
440 administration of magnesium, which is a mild calcium channel blocker (31), is helpful in
441 the acute management of patients with drug-induced *torsades de pointes* (14), and
442 conversely that hypomagnesaemia, which would stimulate I_{CaL}, can exacerbate *torsades de*
443 *pointes* (39). It is also consistent with the observation that drugs that block I_{CaL} and I_{Kr} (e.g.,
444 verapamil) are not associated with drug-induced arrhythmias (40) and that verapamil
445 prevented the development of *torsades de pointes* in rabbit hearts exposed to an I_{Kr} blocker
446 (41). However, given that calcium channel blockers are contra-indicated in some
447 ventricular arrhythmias (42), and the likelihood that patients who have drug-induced
448 LQTS may have other underlying cardiac conditions (14), one should be cautious about
449 prescribing calcium channel blockers. Conversely, it would be reasonable to consider using
450 calcium channel blockers to treat patients with LQTS type 2 (i.e. patients with an isolated
451 loss of I_{Kr} function) who continue to have cardiac events despite treatment with ß-blockers
452 (43).

453 In summary, we have demonstrated that meta-analysis of large-scale gene expression data
454 sets is a powerful technique for discerning underlying patterns in gene expression, and
455 that this can provide insights into disease causation at an individual level. Specifically, we
456 have demonstrated that the co-expression of *KCNH2* (I_{Kr}) and *CACNA1c* (I_{CaL}) plays an
457 important role in regulating cardiac repolarization both in health and in disease.

458

459 **Methods**

460 **Analysis of public RNASeq datasets**

461 An aggregate co-expression gene network was built from public data, similar to that
462 described previously(44). Briefly, 75 human RNA-seq expression experiments (listed in
463 Supp **Table S2**) that passed quality control and had a least 10 samples (3653 samples in
464 total) were downloaded from the Gemma database (45). Approximately thirty thousand
465 genes were used for the network, limited only to those with Entrez gene identifiers. A co-
466 expression network was generated for each experiment by calculating Spearman's
467 correlation coefficients between every gene pair and then ranking these values (44). An
468 aggregate gene co-expression network was then generated by averaging across all the
469 individual networks, and re-ranking the final network. This final aggregate network was
470 then used to determine the co-expression ranking between genes that encode for the set
471 of ion channels and calcium handling proteins that determine the shape and duration of
472 the human ventricular AP, the so-called rhythmonome gene subset (see Supp **Table S1**).
473 Network connectivity of the gene set was measured by comparing the weighted local node
474 degree to the global node degree(46). Node degrees are the sum of the total connections a
475 node (here gene) has within a network. Local node degree refers to the sum of connections
476 (here the ranked correlation) within the rhythmonome gene set, while global node degree

477 is the sum of connections to that gene across all the genes in the network. Code for the
478 analysis is available at https://github.com/sarbal/hERG-cal

479 **Human induced pluripotent stem cell derived cardiac myoctes.**

480 Human iPSC lines, generated from healthy patients by Stanford Cardiovascular Institute
481 Biobank, as previously described (47), were a generous donation from Joseph Wu
482 (Standford Cardiovascular Institute). HiPSC colonies were maintained on Matrigel®
483 (Corning) coated plates in chemically defined medium (mTeSR1™, StemCell technologies),
484 and passaged using Dispase (StemCell technologies). For differentiation, hiPSCs were
485 dissociated by incubating at 37°C for 7 minutes with TrypLE™ Express (ThermoFisher) and
486 seeded at 125000 cells/cm^2 on a Matrigel® coated 12 well plate, in mTeSR™1 medium
487 supplemented with StemMACS™ Y27632 (Miltenyi Biotec). Once the cells reached greater
488 than 95% confluency, differentiation was initiated using STEMdiff™ Cardiomyocyte (CM)
489 differentiation and Maintenance Kit (StemCell technologies). At day 15, CMs were
490 dissociated by incubation in Collagenase Type I (ThermoFisher) for 45 minutes at 37°C to
491 break up the matrix and then incubated in 0.25% Trypsin with EDTA for 7 minutes at room
492 temperature followed by filtering through a 40 µm cell strainer (48). The CMs were seeded
493 on a Fibronectin coated 96-well plate (Greiner Bio-One) and maintained in CM
494 maintenance medium for 10-15 days before they were harvested for mRNA expression
495 analysis. Total RNA was obtained from 40,000 hiPSC-CMs lysed using QIAzol Lysis reagent
496 (Qiagen). The RNA was purified using miRNeasy® Mini Kit (Qiagen), and all samples had
497 RIN values >7.5, and were analysed using Agilent Bioanalyzer pico-chip. RNA samples were
498 hybridised with probes designed to detect 35 known rhythmonome genes using nCounter
499 (NanoString Technologies, see Supplementary **Table S1**), which was performed at the
500 Ramaciotti Centre for Genomics (UNSW).

501 **Computer modelling**

502 Human cardiac APs were simulated using the endocardial configuration of the O'Hara-
503 Rudy (ORD11) model (25) with key conductances modified as described by Krogh-Madsen
504 et al. (26) (See Supp **Figure S1**). The original ORD11 code was adapted to run in the Brain
505 Dynamics Toolbox for Matlab (49). To incorporate population variability in ion channel
506 expression levels the maximum conductance for each current was multiplied by
507 conductance scalar (G_x), that was drawn from a random log-normal distribution (37), with
508 unit mean and variance that was systematically manipulated from 0.05 to 0.5. All models
509 were paced at 1Hz with a stimulus of -40 mV and duration of 1 ms and allowed to
510 equilibrate for 300 beats. We then analysed the next four beats (to allow for the possibility
511 of development of alternans) after the equilibration stage. The peaks in those APs were
512 identified using the Matlab *findpeaks* function. Individual beats were classified as ectopic
513 if they had secondary peaks that were separated by more than 100 ms. The set of four beats
514 were further classified as *alternans* if the profile of any of the APs deviated from each other
515 by more than 1 mV at any time point. In a second set of simulations, we repeated the same
516 method as above except that the random multipliers applied to both I_{CaL} and I_{Kr} were

517 identical. This case we denote co-expression whereas the former case we denote
518 independent expression.
519

520 **Acknowledgements**

521 This work was supported by grants from the National Health and Medical Research Council
522 (NHMRC), App1116948 (to JIV), App1074386 (to JIV), (App1164518 to APH), by the
523 National Institutes of Health (NIH) R01LM012736 (to JAG), R01MH113005 (to JAG), and
524 supported by the Victor Chang Cardiac Research Institute Innovation Centre, funded by the
525 NSW Government. We also thank Terry Campbell, Dan Roden and Raj Subbiah for helpful
526 discussions.
527
528
529 **References**
530

531 1. Zipes DP, Wellens HJ. Sudden cardiac death. Circulation. 1998;98(21):2334–51.

532 2. Behr E, Ensam B. New approaches to predicting the risk of sudden death. Clinical
533 Medicine. 2016;16(3):283–3.

534 3. Jan LY, Jan YN. Voltage-gated potassium channels and the diversity of electrical
535 signalling. J Physiol (Lond). 2012;590(11):2591–9.

536 4. Noble D, Garny A, Noble PJ. How the Hodgkin-Huxley equations inspired the Cardiac
537 Physiome Project. J Physiol (Lond). 2012;590(11):2613–28.

538 5. Marder E, Goaillard J-M. Variability, compensation and homeostasis in neuron and
539 network function. Nat Rev Neurosci. 2006;7(7):563–74.

540 6. Weiss JN, Karma A, MacLellan WR, Deng M, Rau CD, Rees CM, et al. "Good enough
541 solutions" and the genetics of complex diseases. Circ Res. 2012;111(4):493–504.

542 7. Prinz AA, Billimoria CP, Marder E. Alternative to Hand-Tuning Conductance-Based
543 Models: Construction and Analysis of Databases of Model Neurons. J Neurophysiol.
544 2003;90(6):3998–4015.

545 8. Britton OJ, Bueno-Orovio A, Van Ammel K, Lu HR, Towart R, Gallacher DJ, et al.
546 Experimentally calibrated population of models predicts and explains intersubject
547 variability in cardiac cellular electrophysiology. Proceedings of the National Academy
548 of Sciences. 2013;110(23):E2098–105.

549 9. Sarkar AX, Sobie EA. Quantification of repolarization reserve to understand inter-
550 patient variability in the response to pro-arrhythmic drugs: a computational analysis.
551 Heart Rhythm 2011;8(11):1749–55.

552 10. Liberos A, Bueno-Orovio A, Rodrigo M, Ravens U, Hernandez-Romero I, Fernandez-
553 Aviles F, et al. Balance between sodium and calcium currents underlying chronic atrial
554 fibrillation termination_ An in silico intersubject variability study. Heart Rhythm.
555 2016;13(12):2358–65.

556 11. Passini E, Mincholé A, Coppini R, Cerbai E, Rodríguez B, Severi S, et al. Mechanisms of
557 pro-arrhythmic abnormalities in ventricular repolarisation and anti-arrhythmic
558 therapies in human hypertrophic cardiomyopathy. J Mol Cell Cardiol. 2016;96(C):72–
559 81.

560 12. Marder E. Understanding Brains: Details, Intuition, and Big Data. PLoS Biol.
561 2015;13(5):e1002147–6.

562 13. O'Leary T, Sutton AC, Marder E. Computational models in the age of large datasets. Curr
563 Opin Neurobiol. 2015;32:87–94.

564 14. Roden DM. Drug-induced prolongation of the QT interval. N Engl J Med.
565 2004;350(10):1013–22.

566 15. Schulz DJ, Goaillard J-M, Marder EE. Quantitative expression profiling of identified
567 neurons reveals cell-specific constraints on highly variable levels of gene expression.
568 Proceedings of the National Academy of Sciences. 2007;104(32):13187–91.

569 16. Eisen MB, Spellman PT, Brown PO, Botstein D. Cluster analysis and display of genome-
570 wide expression patterns. Proceedings of the National Academy of Sciences. 1998
571 95(25):14863–8.

572 17. Gaiteri C, Ding Y, French B, Tseng GC, Sibille E. Beyond modules and hubs: the potential
573 of gene coexpression networks for investigating molecular mechanisms of complex
574 brain disorders. Genes Brain Behav. 2013;13(1):13–24.

575 18. Rees CM, Yang J-H, Santolini M, Lusis AJ, Weiss JN, Karma A. The Ca2+ transient as a
576 feedback sensor controlling cardiomyocyte ionic conductances in mouse populations.
577 eLife. 2018;7:4417.

578 19. Lee HK, Hsu AK, Sajdak J, Qin J, Pavlidis P. Coexpression analysis of human genes across
579 many microarray data sets. Genome Res. 2004;14(6):1085–94.

580 20. Gillis J, Pavlidis P. The role of indirect connections in gene networks in predicting
581 function. Bioinformatics. 2011;27(13):1860–6.

582 21. Ballouz S, Verleyen W, Gillis J. Guidance for RNA-seq co-expression network
583 construction and analysis: safety in numbers. Bioinformatics. 2015;31(13):2123–30.

584 22. Vandenberg JI, Walker BD, Campbell TJ. HERG K+ channels: friend and foe. Trends
585 Pharmacol Sci. 2001;22(5):240–6.

586 23. Bush WS, Crawford DC, Alexander C, George AL Jr, Roden DM, Ritchie MD. Genetic
587 variation in the rhythmonome: ethnic variation and haplotype structure in candidate
588 genes for arrhythmias. Pharmacogenomics. 2009;10(6):1043–53.

589 24. Sah R, Ramirez RJ, Backx PH. Modulation of Ca 2+Release in Cardiac Myocytes by
590 Changes in Repolarization Rate. Circ Res. 2002;90(2):165–73.

591 25. O'hara T, Virág L, Varró A, Rudy Y. Simulation of the Undiseased Human Cardiac
592 Ventricular Action Potential: Model Formulation and Experimental Validation. PLoS
593 Comput Biol. 2011;7(5):e1002061–29.

26. Krogh-Madsen T, Jacobson AF, Ortega FA, Christini DJ. Global Optimization of Ventricular Myocyte Model to Multi-Variable Objective Improves Predictions of Drug-Induced Torsades de Pointes. Frontiers in Physiology. 2017;8:e1000173–10.

27. Sayed N, Liu C, Wu JC. Translation of Human-Induced Pluripotent Stem Cells. J Am Coll Cardiol. 2016;67(18):2161–76.

28. Robertson C, Tran DD, George SC. Concise Review: Maturation Phases of Human Pluripotent Stem Cell-Derived Cardiomyocytes. Stem Cells 2013;31(5):829–37.

29. Pedersen HS, Elming H, Seibæk M, Burchardt H, Brendorp B, Torp-Pedersen C, et al. Risk Factors and Predictors of Torsade de Pointes Ventricular Tachycardia in Patients With Left Ventricular Systolic Dysfunction Receiving Dofetilide. Am J Cardiol. 2007;100(5):876–80.

30. Shimizu W, Moss AJ, Wilde AAM, Towbin JA, Ackerman MJ, January CT, et al. Genotype-phenotype aspects of type 2 long QT syndrome. J Am Coll Cardiol. 2009;54(22):2052–62.

31. Hartzell HC. Effects of magnesium on inactivation of the voltage-gated calcium current in cardiac myocytes. J Gen Physiol. 1989;94(4):745–67.

32. Marder E, Goaillard J-M. Variability, compensation and homeostasis in neuron and network function. Nat Rev Neurosci. 2006;7(7):563–74.

33. Bányász T, Horváth B, Jian Z, Izu LT, Chen-Izu Y. Sequential dissection of multiple ionic currents in single cardiac myocytes under action potential-clamp. J Mol Cell Cardiol 2011;50(3):578–81.

34. Min B, Zheng M. Correlated network of networks enhances robustness against catastrophic failures. PLoS ONE. 2018;13(4):e0195539–13.

35. The QT Interval International GWAS Consortium (QT-IGC), Lundby A, Rossin EJ, Steffensen AB, Acha MR, Newton-Cheh C, et al. Annotation of loci from genome-wide association studies using tissue-specific quantitative interaction proteomics. Nat Methods 2014;11(8):868–74.

36. Huang CL-H. Murine Electrophysiological Models of Cardiac Arrhythmogenesis. Physiol Rev. 2017;97(1):283–409.

37. Sadrieh A, Mann SA, Subbiah RN, Domanski L, Taylor JA, Vandenberg JI, et al. Quantifying the origins of population variability in cardiac electrical activity through sensitivity analysis of the electrocardiogram. J Physiol (Lond) 2013;591(17):4207–22.

38. Marder E. Variability, compensation, and modulation in neurons and circuits. Proceedings of the National Academy of Sciences. 2011;108(Supplement_3):15542–8.

39. Roden DM, Iansmith DH. Effects of low potassium or magnesium concentrations on isolated cardiac tissue. The American Journal of Medicine. 1987;82(3A):18–23.

40. Redfern WS, Carlsson L, Davis AS, Lynch WG, MacKenzie I, Palethorpe S, et al. Relationships between preclinical cardiac electrophysiology, clinical QT interval

632 prolongation and torsade de pointes for a broad range of drugs: evidence for a
633 provisional safety margin in drug development. Cardiovasc Res. 2003;58(1):32–45.

634 41. Farkas AS, Makra P, Csík N, Orosz S, Shattock MJ, Fülöp F, et al. The role of the
635 Na+/Ca2+ exchanger, INa and ICaL in the genesis of dofetilide-induced torsades de
636 pointes in isolated, AV-blocked rabbit hearts. Br J Pharmacol. 2009;156(6):920–32.

637 42. Akhtar M, Tchou P, Jazayeri M. Use of calcium channel entry blockers in the treatment
638 of cardiac arrhythmias. Circulation 1989;80(6 Suppl):IV31–9.

639 43. Komiya N, Tanaka K, Doi Y, Fukae S, Nakao K, Isomoto S, et al. A patient with LQTS in
640 whom verapamil administration and permanent pacemaker implantation were useful
641 for preventing torsade de pointes. Pacing and Clinical Electrophysiology.
642 2004;27(1):123–4.

643 44. Ballouz S, Verleyen W, Gillis J. Guidance for RNA-seq co-expression network
644 construction and analysis: safety in numbers. Bioinformatics. 2015;31(13):2123–30.

645 45. Zoubarev A, Hamer KM, Keshav KD, McCarthy EL, Santos JRC, Van Rossum T, et al.
646 Gemma: a resource for the reuse, sharing and meta-analysis of expression profiling
647 data. Bioinformatics. 2012;28(17):2272–3.

648 46. Ballouz S, Gillis J. Strength of functional signature correlates with effect size in autism.
649 Genome Med. 2017;9(1):64.

650 47. Burridge PW, Diecke S, Matsa E, Sharma A, Wu H, Wu JC. Modeling Cardiovascular
651 Diseases with Patient-Specific Human Pluripotent Stem Cell-Derived Cardiomyocytes.
652 Methods Mol Biol.; 2016;1353(Chapter 196):119–30.

653 48. Mills RJ, Titmarsh DM, Koenig X, Parker BL, Ryall JG, Quaife-Ryan GA, et al. Functional
654 screening in human cardiac organoids reveals a metabolic mechanism for
655 cardiomyocyte cell cycle arrest. Proceedings of the National Academy of Sciences.
656 2017;114(40):E8372–81.

657 49. Heitmann S, Aburn MJ, Breakspear M. The Brain Dynamics Toolbox for Matlab.
658 Neurocomputing; 2018;315:82–8.

659